

PHYS 4991: Summarizing My Research on X-ray Binaries Comprising Spectral Analysis and Involvement in the Development of Source Catalogues

April Walker

University of Arkansas, Fayetteville

*Submitted in partial fulfillment of the requirements for PHYS 4991 and the
Fulbright College Senior Writing Requirement.*

In this paper I will discuss my involvement in research regarding the formation and evolution of x-ray binaries. Using observations from the *Chandra X-ray Observatory*, I helped develop a source catalogue of processed data for 16 early type galaxies for a study of the variation of the x-ray luminosity function in field low mass x-ray binaries. My involvement included developing exposure maps, point source function maps, and images to be further analyzed by my research professor Dr. Bret Lehmer to develop a catalogue. For use in a different study, I then developed script to bin data from numerous x-ray observations in various galaxies in order to do a spectral analysis. Currently, I am working on developing models with which I can fit the data. Due to the nature of this paper and in order to make this paper more accessible to the layman, I have developed a table in the appendix giving a brief description of astronomical keywords used in this paper.

1 Introduction: X-ray Binaries and their Research Applications

Due to *Chandra X-ray Observatory's* high resolution imaging capabilities, our understanding of the evolution and formation of compact objects has been profoundly impacted. With its sub-arcsecond resolution images, we have been able to study x-ray objects in extragalactic environments at revolutionary distances. With such a sample size to study x-ray binary (XRB) populations, incredible advances in our knowledge of the evolution of the objects and properties which they contain (e.g. compact objects^{11, 9}, accretion dynamics²) have been achieved. Furthermore, you can learn more about the descendants of some XRBs such as Supernovae (SNe) and millisecond pulsars⁹. While this knowledge in its own right impacts our understanding of our Universe, XRB research could potentially provide indirect insight into the evolution of galaxies through the study of accretion dynamics².

Our current accepted gravitational theory, Einstein's Relativity, necessitates that speed of light in a vacuum is an absolute physical constant. This finite nature of light allows astronomers to study the evolution of stellar structures on a cosmic time scale. By discovering how various properties change with the evolution of a stellar object, galaxy, or the Universe, we can determine how specific properties impact the likelihood of various phenomenon, including the nature of x-ray binaries (XRB) populations⁹.

An XRB is a luminous x-ray emitting binary system consisting of one "donor" star and one "accretor" compact object of which matter from the donor flows into. In the language of astronomy, compact object refers to a massive compact stellar objects such as white dwarfs, neutron stars, and black holes. Falling in line with angular-momentum conservation, matter transferring from the "donor" to the "accretor" settles in an accretion disk. As a result of their massive but compact quality, space-time is severely distorted, and accretion dynamics becomes increasingly complex upon reaching "accretor" in this binary system. By studying XRBs, a unification of theory and observation can lead to robust model of accretion flow in extreme gravitational environments². In other words, by understanding the nature of accretion

flow in XRBs one can apply those findings to larger scales, such as the black hole present in the active galactic nucleus (AGN) of most galaxies. Observational evidence shows the growth of a galaxy correlates with the growth of its AGN. A growing body of evidence is showing that this growth mechanism is intimately linked with to feedback from accretion flow. Due to this, increased apprehension of XRB accretion could have significance in deepening our understanding of galactic evolution ².

While we know XRB formation is sensitive to properties such as metallicity and age of the parent stellar population, determining how the x-ray luminosity function (XLF) evolves in a stellar population is a matter of current research ^{9, 12}. On it's own, a deeper understanding of the XLF can lead to a more through understanding of the evolution and formation of x-ray binaries. Star formation history is one of various properties which impacts XRB formation. Although more indirect, understanding XRB populations could also further our understanding of star formation rates. X-ray emission is generally a tell-tale signature of AGN activity in galaxies. However, x-ray emission is also produced by young stellar populations containing XRB's. In the absence of XRBs, the correlation between star formation rate (SFR) and x-ray luminosity becomes more clear. While determining star formation rate with x-rays overcomplicates the problem due to the variability of XRBs, A robust understanding of the XLF could provide a quantifiable reason for this disconnect between SFR and x-ray emissions ¹⁴.

X-ray emissions of XRBs are anything but steady. This fluctuations differs from object to object, therefore parameterizing which variables impact x-ray emission; determining the extent of their impact is necessary to understanding XRBs. In addition to typical thermal x-ray emission from accretion disks, XRBs emit a power-law spectrum of hard x-rays and sometimes gamma-rays. This is due to the Compton scattering of softer x-rays leading to a decrease in energy of the photon. If the XRB is thermally dominated, it is considered to be in a high/soft state. Alternatively, the XRB could be in a power-law dominated low/hard state^{1,2,5}. However, this is a very simplistic and inaccurate representation of the various states of an XRB^{1,5}, and will be discussed further in section 3. .

The interesting properties of x-ray binaries make it a stellar object of recognizable interest to astronomical research. By studying the evolution and formation of x-ray binaries, one can learn about the galaxy which contains them. Beyond this, the compact nature of these objects allows us to learn about similar less numerous objects such as super massive black holes within the AGN. Improvements in our understanding of x-ray binaries provide insight into questions regarding galactic evolution and even our cosmic history.

2 Development of *Chandra* Source Catalogue of Early-type Galaxies for Measurement of Field Low Mass X-ray Binary Populations

In our own galaxy, the Milky Way (MW) galaxy, low mass XRBs (LMXBs) are the most numerous. Current evidence leads us to believe that LMXBs have dominated normal galaxy emissivity of the Universe since $z \approx 2^{7,4}$. Formation of LMXB's occurs in two general ways: (1) Through the overflow of a normal star's Roche-lobe onto a compact object isolated within the galactic field's they formed or (2) through dynamic interactions within stellar cluster due to the gravitational binding of the stellar population⁸.

Globular clusters provide an ideal birthplace for LMXB's, and therefore the formation mechanism behind GC LMXB has been thoroughly studied by previous research^{13,7}. The formation mechanism of field LMXB's mentioned, on the other hand, have yet to be determined in detail. Like GC LMXB, it is theorized variables such as metallicity and the stellar population age and star formation rate impact the rate of field LMXB formation⁴. Other considerations are whether it's possible GC environments provide a birthplace for field LMXB populations. The LMXB's new galactic environment could be due to the dissolution of evolved star clusters or the ejection of the LMXB from its place of origin⁸.

This study therefore aims to combine *Chandra*'s high resolution capabilities with Hubble's counterpart images providing morphological information to determine whether the LMXB is within the field, a GC, or merely a background observation. Using this, this study aims to

determine specifically the formation mechanism of field LMXBs. The more goal of this study is to further our understanding of the evolution of compact objects, accretion dynamics, and how their populations vary throughout the cosmos⁸.

Previous to this study, a pilot study involving 3 early type galaxies varying over $\approx 3 - 10$ Gyrs was completed. This study found that the "young" early-type galaxy NGC 3384 contained excessive luminous field LMXB's when compared to the older galaxies NGC 3315 and 3379. However, to determine with statistical accuracy how the x-ray luminosity function (XLF) changes as a galaxy ages, a more in depth study must be done. In order to do so, early-type galaxies spanning $\approx 2 - 13$ Gyrs were chosen. Using a base sample of 376 nearby early-type galaxies by Ellis & O'Sullivan (2006)³, 16 were narrowed down based off the capabilities of both *Chandra* and *Hubble* to provide clear imaging such that field LMXBs would be distinguishable. Below, Table 2 gives the properties of the 16 galaxies chosen for the follow up study. For further data, within the appendix is a Figure 1A comparing the approximate age span of the galaxies chosen for the pilot study and that of the galaxies chosen for the follow up robust study.

Table 1. Summary of Galaxy Samples and Properties

| Gal (1) | D (Mpc) (2) | Age (Gyr) (3) | S_N (4) | a (arcmin) (5) | b (6) | $\log L_K$ ($L_{K,\odot}$) (7) | $\log L_X^{90}$ (erg s^{-1}) (8) | Num. LMXBs N_{field} (9) | N_{GC} (10) | <i>Chandra</i> (ks) (11) | <i>Hubble</i> g (12) | Coverage z (13) |
|--------------|---------------------|---------------------|--------------|------------------------|------------|--|---|---|--------------------------------|--------------------------------|------------------------------|-------------------------|
| N4382 | 17.1 | 1.7 ± 0.3 | 1.3 | 4.2 | 2.8 | 11.4 | 37.9 | 18 ± 4 | 11 ± 3 | 60 | F475W | F814W |
| N3585 | 18.2 | 3.1 ± 1.0 | 1.3 | 3.0 | 1.9 | 11.2 | 37.7 | 19 ± 4 | 9 ± 3 | 96 | F475W | F850LP |
| N3384 | 11.5 | 3.2 ± 1.5 | 1.1 | 3.6 | 1.8 | 10.7 | 37.2 | 19 ± 4 | 4 ± 2 | 133 | F475W | F850LP |
| N3923 | 19.1 | 3.3 ± 0.8 | 6.8 | 3.8 | 2.5 | 11.4 | 37.7 | 28 ± 5 | 70 ± 8 | 102 | F606W | F814W |
| N1404 | 18.7 | 5.9 ± 1.0 | 1.7 | 2.5 | 2.2 | 11.3 | 37.0 | 97 ± 9 | 28 ± 5 | 535 | F475W | F814W |
| N4621 | 18.2 | 6.9 ± 3.9 | 2.7 | 3.4 | 2.2 | 11.1 | 38.2 | 2 ± 1 | 7 ± 2 | 30 | F475W | F850LP |
| N3115 | 9.6 | 8.5 ± 0.9 | 2.3 | 4.2 | 1.6 | 10.9 | 36.1 | 151 ± 12 | 23 ± 4 | 1113 | F475W | F850LP |
| N3379 | 10.5 | 8.6 ± 0.9 | 1.3 | 3.2 | 2.7 | 10.8 | 36.7 | 51 ± 7 | 9 ± 3 | 333 | F475W | F850LP |
| N4552 | 15.3 | 8.9 ± 1.0 | 2.8 | 3.3 | 3.1 | 11.0 | 37.2 | 33 ± 5 | 19 ± 4 | 201 | F475W | F850LP |
| N4374 | 18.3 | 10.4 ± 1.0 | 5.2 | 3.8 | 3.5 | 11.3 | 37.6 | 29 ± 5 | 47 ± 6 | 117 | F475W | F850LP |
| N4649 | 16.8 | 11.0 ± 1.0 | 5.2 | 4.0 | 3.3 | 11.4 | 37.1 | 100 ± 10 | 98 ± 9 | 308 | F475W | F814W |
| N4697 | 11.7 | 11.0 ± 1.2 | 2.5 | 4.0 | 2.5 | 10.9 | 37.0 | 38 ± 6 | 17 ± 4 | 193 | F475W | F814W |
| N4278 | 16.0 | 11.6 ± 1.1 | 6.9 | 2.6 | 2.4 | 10.8 | 36.8 | 42 ± 6 | 43 ± 6 | 580 | F475W | F850LP |
| N4472 | 16.2 | 12.5 ± 1.0 | 5.4 | 5.2 | 4.2 | 11.5 | 36.9 | 180 ± 13 | 157 ± 12 | 470 | F475W | F850LP |
| N4365 | 20.4 | 12.6 ± 1.1 | 3.9 | 3.4 | 2.5 | 11.2 | 37.5 | 31 ± 5 | 32 ± 5 | 196 | F475W | F850LP |
| N4473 | 15.7 | 13.2 ± 4.0 | 2.0 | 2.9 | 1.6 | 10.8 | 38.1 | 2 ± 1 | 3 ± 1 | 30 | F475W | F850LP |
| Total | | | | | | | | 840 ± 28 | 577 ± 24 | 4.5Ms | | |

Note. — Col.(1): Galaxy name. Col.(2): distance in Mpc. Col.(3): Stellar age taken in order of priority from Sánchez-Blázquez et al. (2006), McDermid et al. (2006), Terlevich & Forbes (2001), and Thomas et al. (2005). Col.(4): Specific frequency. Col.(5)–(6): major and minor axes. Col.(7): K -band luminosity. Col.(8): Estimated 90% complete 0.5–8 keV detection limit. Col.(9) and (10): Expected number of LMXBs detected down to L_X^{90} for field and GC LMXBs, respectively (see footnote 2 for details). Col.(11): Archival *Chandra* exposure available. Col.(12) and (13): Equivalent g and z -band data available from *Hubble* archive.

In order to analyze data from *Chandra*, the raw data must be processed; images, exposure maps, and point source function (PSF) maps had to be developed. In order to do this, raw data of all clear observations available for a given galaxy was downloaded and processed using a series of Shell scripts which incorporated CIAO, a data analysis software developed to analyze data from the *Chandra X-ray Observatory*. My main input into this portion of the research involved automating scripts such that data could quickly be processed for each observation. Because the script developed for the pilot study did not require extensive use, automation was not considered. This meant the user would need to personally go through the lines of script and replace file names to those for a specific observations.

This portion of my research involving the automation of scripts was done in conjunction with another member of my research group, Larissa Markwardt, who is currently a graduate student at the University of Michigan. The finished product was written in *Bash/Shell*, however due to the nature of the languages they are basically interchangeable, as Bash stands for **B**ourne **A**gain **S**hell. Generally, the only change necessary is the environmental variable generally labeled `#!/bin/bash` or similar at the top of ones script. This is called the shebang line, and follow the format `#!/interpreter [optional-argument]`. If you are using a UNIX environment, you can determine which Shell to point to, by typing `printenv SHELL` in the terminal. My specific Shell is `zsh` (or `oh-my-zsh`), as the bash version on my system was incompatible with CIAO.

Related to this issue, a common issue newcomers run into when attempting to run script is environment variables. Even if you attempt to unify the file system naming convention of a research group, it is likely your researcher will find their script doesn't run. A well written code will document which environmental variables need to be set. There are two ways to specify environmental variables: (1) specify the variable immediately before execution of the script by entering into the command line something along the lines of `MY_ENV_VAR="path/to/env/var"` (2) using your terminal text editor of choice (e.g nano, vim), hard code the variable into your bash file (most likely `./bashrc`) by adding something

along the lines of `export MY_ENV_VAR="path/to/env/var"`. You will need to restart your terminal before the new environment variable becomes usable, or type `source ~/.bashrc` (or your bash equivalent) to force your current session to read the file. Beyond the use in scripting, environment variables are very helpful if you often navigate the command line during your research.

A key aspect of the scientific process is repeatable methodology. As science progresses and becomes increasingly dependent on computers, it will become increasingly necessary to document changes and methods used to develop a finished product. Beyond the importance of reproducible data, ignoring issues such as documentation and version control leads to technological debt. While technological short-cuts may allow you to get the data you need in the short run, the debt adds up and will end up slowing down the research process in the long run. In regards to software development, version control means controlling the main codebase or repository by requiring certain steps to be taken before pushing code into production. This can be achieved using git or similar software. If you're okay with your software being made public, you can use online services such as GitHub to both allow for version control and backup your repository.

In regards to my own project, version control was the major issue concerning collaboration with my research associate. Some work on script was repeated by both of us, as communication regarding script automation was generally achieved via e-mail. Moving forward into my research project discussed in Section 3, I instead used an offline repository to allow myself to change code. This came in handy when my project branched to compare the results of differing analysis methods.

Each script was automated and tested using one of the galaxies from the pilot study, NGC 3384. It was an ideal candidate as the images, PSF maps, and exposure maps developed using our automated scripts should be identical to those produced in the pilot study. In addition, other research in our group had also analyzed this galaxy, therefore giving us a large body of data to compare with. At this point my collaboration stopped, and I remained in charge

of developing the appropriate maps and images for the remaining galaxies listed in Table 2. I continued by processing the last 2 galaxies within the pilot study, and then processed data for the last 13.

The data was developed as follows. Once all data is downloaded from the *Chandra* Data Archives and put in the appropriate folder, the script `analyze-all-auto.sh` was run. This script must first be run using the observation with the longest exposure, as preceding observations are compared with the first to adjust the position of aspect and event files using the CIAO commands `reproject_aspect` and `reproject_events` respectively. This script develops temporary images and PSF maps from the raw data, and then runs `wavdetect` in order to provide an initial catalog with image files, PSF maps, and exposure maps. Light curves are constructed and then checked for points of error, such as periods of excessively high or low count rates. This is accomplished using the CIAO command `deflare`.

Next the `construct_merged_auto.sh` script was ran to develop images, PSF maps, and exposure maps for specific keV bands for each observation, as well as a final merged version. These include "0.5-2" which specifies soft x-ray keV band, "2-7" which specifies hard x-ray keV band, and lastly "0.5-7" which specifies the full *Chandra* keV band. This script asks that you specify each observation for a given galaxy, as this script must be run on all observations at once in order to provide a robust final product. By running this script, one initiates another script `create_merged_lists.script`. This more minimal script develops a list of files of each observation in a galaxy which must be combined using the CIAO command `merge_obs`.

The final product was a collection of exposure maps and PSF maps spanning across particular portions of the keV band, as well as a final merged image in the form of a FITS file. Below is an example of such data as gathered from NGC 4697. In the middle is the final merged image, the right contains the exposure map for the full band keV, and the left contains the PSF map for the full band keV. The image is colored to "hsv" in *DS9* (visualization software for astronomical images such as FITS and binary files) to make it more viewable to the reader.

Although not very clear in such a faint galaxy, this image was developed in conjunction with the exposure maps and PSF maps.

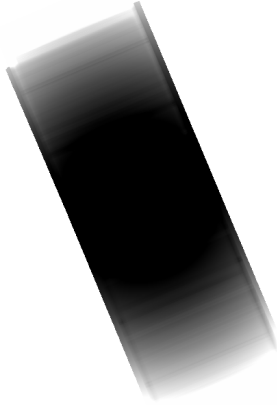


Fig. 1. PSF Map for NGC 4697



Fig. 2. Merged Image for NGC 4697

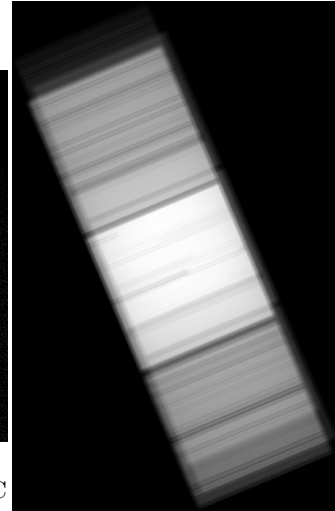


Fig. 3. Exposure Map for NGC 4697

In order to compare to individual observations, below is an image (middle), exposure map (right), and PSF map (left) for a single observation of NGC 4697.

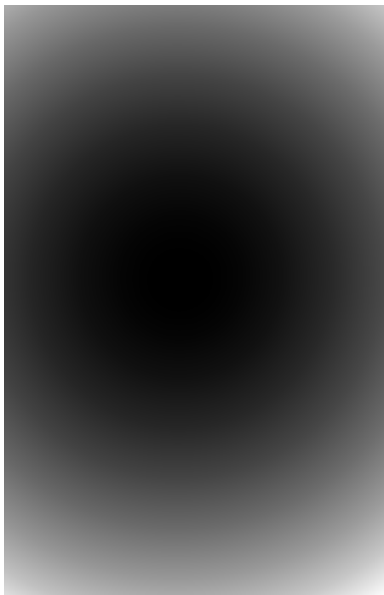


Fig. 4. PSF Map for single NGC 4697 observation

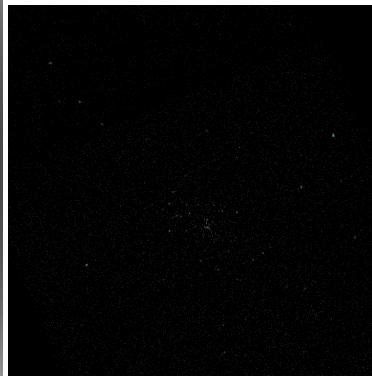


Fig. 5. Merged image for single NGC 4697 observation

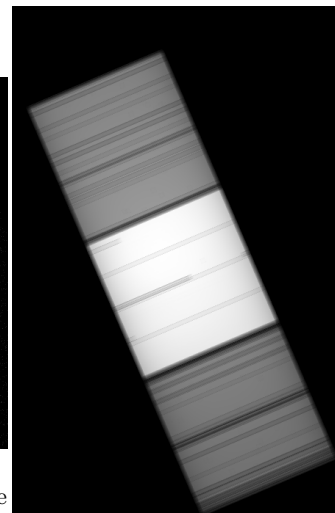


Fig. 6. Exposure map for single NGC 4697 observation

The overlap of each exposure map for NGC 4697 makes it difficult to distinguish between observations in the final product. In order to more adequately show the diversity of results achieved from this research, I have added additional exposure maps in the appendix.

Once my collection of maps and images for the 16 galaxies was complete, I passed on my research to my professor who further analyzed the data the data for use in the robust study of field LMXBs.

3 Data Binning and Spectral Analysis:

As discussed in section 1, x-ray emissions of XRBs fluctuates heavily. The emissions of an XRB can be simplified by analyzing the shape of the spectrum and describing it as "soft" or "hard". Below is an image adapted from Gierliński et al(1999)⁵ by Done et al (2007)² characterizing these differences. Here the red is equivalent to a soft state and blue is equivalent to a hard state. This graph was developed from the study of a black hole binary Cyg-X-1.

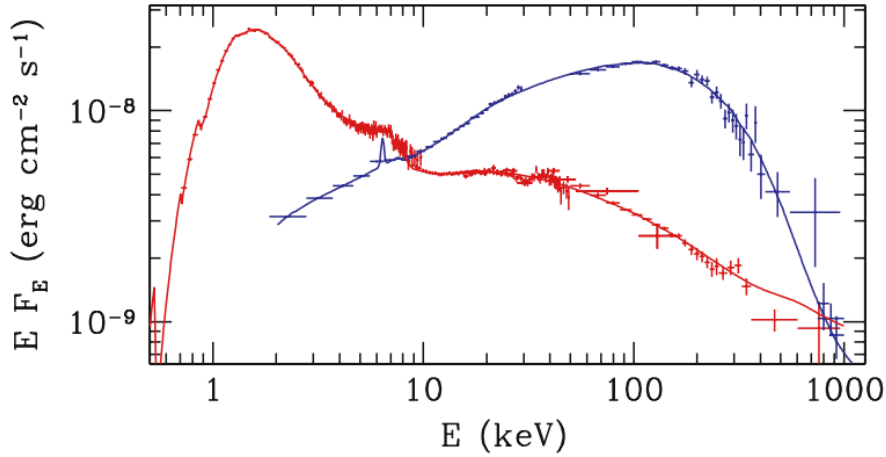


Fig. 7. Spectral states of Cyg X-1 observed in by the *Ginga* satellite and OSSE in 1991

The existence of these two states can be explained by the existence of two unique accretion flow structures. In a soft state, accretion can be modeled with a standard optically thick gaseous disc in which emissions produced can mostly be explained by a soft black-body radiation. The tail preceding can be modeled by a weak but steep power law in which photon

index $\Gamma \approx 2.5$ In it's hard state, the XRBs accretion disc is replaced with an optically thin in $\Gamma \approx 1.6 - 1.8$.⁵ This shift is explained by the Compton scattering of softer x-rays in a flowing accretion of very hot electrons. In this state there are fewer photons illuminating flow within the disc, therefore Compton cooling is overwhelmed by the heating due to collisions with protons.²

This study by Gierliński et al(1999) actually modeled a third intermediate state, and further research has shown the existence of many transition states. Below (left) a graph in Done et al (2007) gives the spectral shape of these various states².

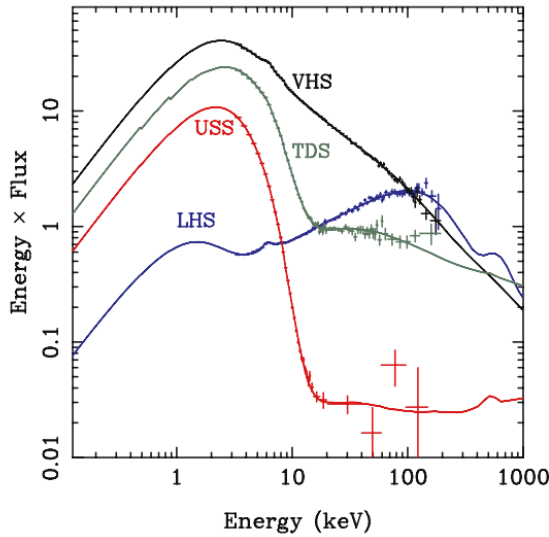


Fig. 8. Spectral states as taken from outburst of GRO J1655-40

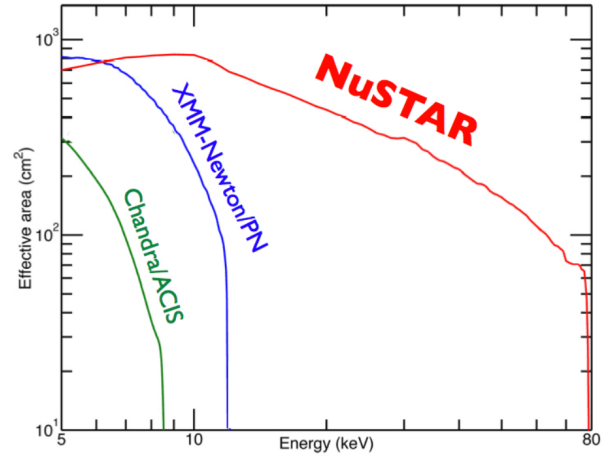


Fig. 9. Comparison of effective area of

Due to *Chandra's* effective area, it can be useful when studying sources at lower intensities. By using *Chandra*, one can pinpoint what types of accretion states are expected. Specifically, the majority of data from *Chandra* should be at the point of the spectrum where soft and like-soft states flux nosedives, and low/hard observations dominate. Above on the right, I give a graph showing the effective area of *Chandra*, *XMM*, and *NuSTAR* as taken from the *NuSTAR* website⁶.

As stated above, the expected photon index Γ for an XRB in a low hard state is $\Gamma \approx 1.6 - 1.8$. In order to compare this with observed data, I used Python to load, organize, and bin data. This also involved systematic deletion of invalid data in order to develop an accurate final product.

For my spectral analysis, I first used analyzed data from NGC 4382 to develop a graph containing all source data and their error bars. However, for a single source, massive error bars prevented a cohesive picture to be formulated. In order to get around this, data was binned together and error was calculated using the following equation:

$$\mu_{err} = \frac{\sqrt{\sum_{i=1}^n x_{err}^2}}{\sqrt{n}}$$

Here, μ_{err} is the mean error of the data points in a bin, x_{err} is the error of a single observation, and n is the number of observations in a bin. However, binning data requires a large data set. Over time, my galaxy source catalogue grew to the 13 galaxies shown in my final graph. In order to quickly load new data in, the following script was developed to open source files of all data within a specific directory. As discussed in Section 2, I make use of environmental variables to reduce the path size name within the script.

```
#set to the directory containing all data you wish to plot
fits_dir = os.listdir(os.environ["RESEARCH_DATA_PATH"] + "/Final-fits/")

#specify the path each data file
for i in range(len(fits_dir)):
    fits_file.append(os.environ["RESEARCH_DATA_PATH"] + "/Final-fits/" + fits_dir[i])
```

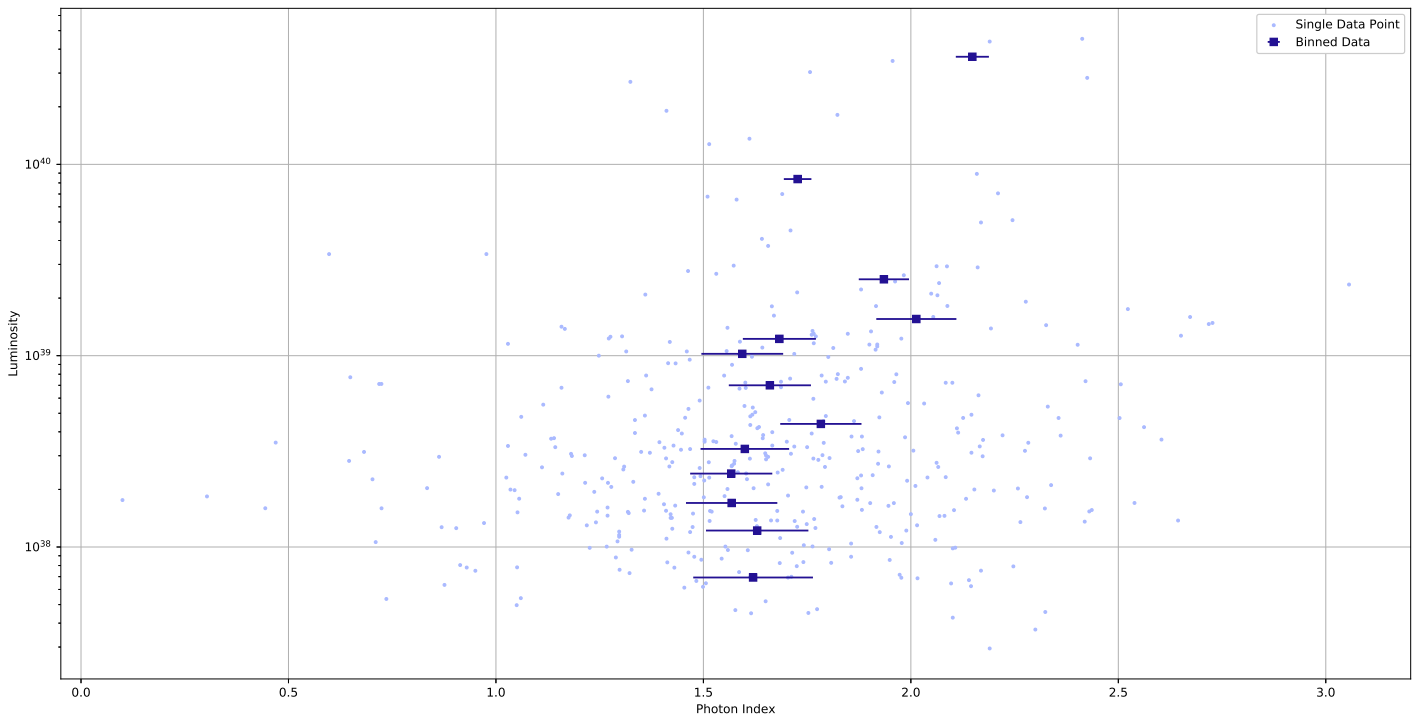
Before binning, the data array was sorted from smallest value to largest using `data_set.sort(key=lambda x: x[0])` where x is equivalent to photon index (Γ) and `data_set` is a coupled array of photon index (Γ), photon index error (Γ_{err}), and luminosity. At this point,

data was binned and error was calculated using algorithm similar to the following pseudocode:

```
j = 0
for i in range(len(data_set)):
    if(exists two binned datapoint):
        if((error value is low enough) and (bin minimum is met)):
            j += 1 #start a new bin
        elif(bin maximum is met):
            j += 1 #start a new bin
        else:
            keep binning
    else:
        add datapoint to the bin
```

The full code of my program can be found in the appendix and begins with the comment
THE BELOW CODE AUTOBINS NORMALLY #. Using this code, the following graph was developed.

Fig. 10. Luminosity vs Photon Index (Γ) of NGC4382, NGC0628, NGC2403, NGC6946, NGC7793, NGC2841, NGC3184, NGC3198, NGC4559, M63, M94, M95, and M100



This graph shows findings consistent with findings from previous studies that show photon index $\Gamma \approx 1.6 - 1.8$. As luminosity increases, the photon seems to shift towards higher values,

however the average remains near $\Gamma \approx 1.7$. Additional graphs comparing binned data from different galaxies can be found in the appendix.

Currently, I am using XSPEC to model the expectation of the data and fit the data to the models. XSPEC allows the user to develop models from simulated data of spectra using the command `fakeit`, or form theoretical models of data using `model` or `mo` (interchangeable in practice). In the context of my project, I can use the power law model `po` in conjunction with various parameters in order to develop a model. I plan on continuing this research over the summer to further current understanding of accretion and spectral states in XRBs.

References:

1. Belloni, T., Homan, J., Casella, P., Klis, M. V., Nespoli, E., Lewin, W. H., . . . Méndez, M. (2005). The evolution of the timing properties of the black-hole transient GX 339–4 during its 2002/2003 outburst. *Astronomy & Astrophysics*, 440(1), 207–222.
2. Done, C., Gierliński, M., Kubota, A. (2007). Modelling the behaviour of accretion flows in X-ray binaries. *The Astronomy and Astrophysics Review*, 15(1), 1–66.
3. Ellis, S. C. and Ewan O’Sullivan (2006). Correlations of near-infrared, optical and X-ray luminosity for early-type galaxies. *RAS, MNRAS* 367, 627–645.
4. Fragos, T., Lehmer, B., Tremmel, M., Tzanavaris, P., Basu-Zych, A., Belczynski, K., . . . Zezas, A. (2013). X-Ray Binary Evolution Across Cosmic Time. *The Astrophysical Journal*, 764(1), 41.
5. Gierlinski, M., Zdziarski, A. A., Poutanen, J., Coppi, P. S., Ebisawa, K., Johnson, W. N. (1999). Radiation mechanisms and geometry of Cygnus X-1 in the soft state. *Monthly Notices of the Royal Astronomical Society*, 309(2), 496–512.
6. Kim, Y., Willis, J., Dodd, S., Harrison, F., Forster, K., Craig, W., . . . Oberg, D. (2013). Nuclear Spectroscopic Telescope Array (NuSTAR) Mission. 2013 IEEE Aerospace Conference.
7. Kundu, A., Maccarone, T. J., Zepf, S. E. (2007). Probing the Formation of Low-Mass X-Ray Binaries in Globular Clusters and the Field. *The Astrophysical Journal*, 662(1), 525–543.
8. Lehmer, B. A First Robust Measurement of the Aging of Field Low Mass X-ray Binary Populations from Hubble and Chandra. Proposal.
9. Lehmer, B. D., Berkeley, M., Zezas, A., Alexander, D. M., Basu-Zych, A., Bauer, F. E., . . . Yukita, M. (2014). The X-Ray Luminosity Functions Of Field Low-Mass X-Ray Binaries In Early-Type Galaxies: Evidence For A Stellar Age Dependence. *The Astrophysical Journal*, 789(1), 52.
10. Madau, P. (2013). Cosmic star formation history. *Annual Review of Astronomy and Astrophysics*, 1056–8700(97), 0610–00.
11. Matteo, T. D., Springel, V., Hernquist, L. (2005). Energy input from quasars regulates the growth and activity of black holes and their host galaxies. *Nature*, 433(7026), 604–607
12. Ranalli, P., Comastri, A., Setti, G. (2005). The X-ray luminosity function and number counts of spiral galaxies. *Astronomy & Astrophysics*, 440(1), 23–37.
13. Sivakoff, G. R., Jordan, A., Sarazin, C. L., Blakeslee, J. P., Cote, P., Ferrarese, L., . . . Peng, E. W. (2007). The Low-Mass X-Ray Binary and Globular Cluster Connection in Virgo Cluster Early-Type Galaxies: Optical Properties. *The Astrophysical Journal*, 660(2)
14. Vattakunnel, S., Tozzi, P., Matteucci, F., Padovani, P., Miller, N., Bonzini, M., . . . Xue, Y. Q. (2012). The radio-X-ray relation as a star formation indicator: Results from the Very Large Array-Extended Chandra Deep Field-South. *Monthly Notices of the Royal Astronomical Society*, 420(3), 2190–2208. doi:10.1111/j.1365-2966.2011.20185.x

Appendix:

Table 1: Keywords, Acronyms, and their Descriptions

| Keyword/Acronym | Acronym | Brief description |
|---------------------------|-----------------------|---|
| Milky Way Galaxy | MK | Our galactic home, a barred spiral galaxy around 100-180 thousand light-years in diameter and estimated to have around 100-400 billion stars. |
| Active Galactic Nucleus | AGN | The compact region at the center of active galaxies which emits excessively across much of the electromagnetic spectrum including radio, near-optical, optical, x-ray, and gamma ray. |
| X-ray Binary | XRB | Luminous x-ray emitting binary system with one "donor" star and one "accretor" compact object of which matter from the donor flows into. |
| Low Mass X-ray Binary | LMXB | The most numerous of XRB's which generally contain a main sequence, white dwarf, or red giant donor which is less massive than the compact object. |
| X-ray Luminosity Function | XLF | A function related to the power law which quantifies how x-ray luminosity varies. It is important to our understanding of the evolution and formation of x-ray emitting objects. |
| Globular Cluster | GC | Collections of stars tightly bound by gravity. Generally in the halo of a galaxy and quite old. |
| GC LMXB | N/A | LMXB's which form in highly dense stellar environments such as globular clusters. The gravitational bind of the local stellar population leads to dynamic interactions between stellar objects. |
| Supernova(e) | SN or SNe | The last evolutionary stage of a massive star's life in which an incredible explosion generally leaving as a remnant a compact object |
| Compact Object | N/A | Massive compact stellar objects such as white dwarfs, neutron stars, black holes. |
| Redshift | z | Quantified by comparing the observed and emitted wavelength (λ) using the equation $z = \frac{\lambda_{obs} - \lambda_{emit}}{\lambda_{emit}}$, redshift is considered the stretching of light due to the expansion of the universe. Therefore, it can be a way to specify time in extragalactic environments. |
| Eddington Luminosity | N/A | Also called the Eddington limit. In order for the force of radiation to be in balance with the gravitational force of the object (hydrostatic equilibrium), it must be less luminous than this value. |
| Compton scattering | N/A | The scattering of a photon by a charged particle, which results in a decrease in energy in the photon. |
| XRB Spectral States | N/A | Accretion activity in XRBs can be described in the terms of shifts in the relationship between x-ray emission and luminosity. These can be roughly categorized by power law dominated "hard" state and a thermal emission dominated "soft" state. |

Below are the merged exposure (right) and PSF maps (left) of the 0.5-7 keV band developed from NGC 3384.

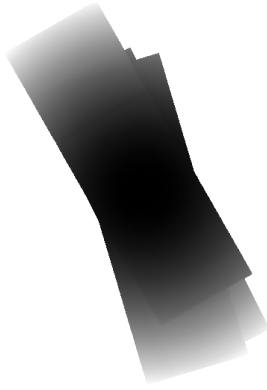


Fig. 11. PSF Map for NGC 3384

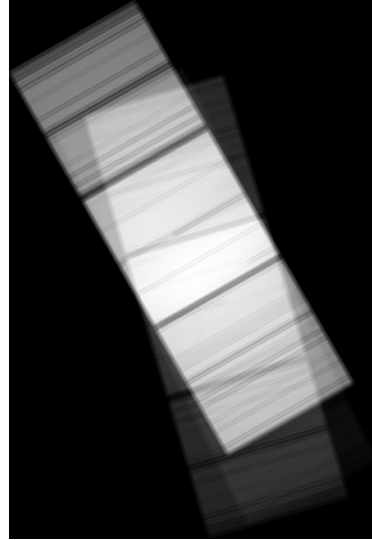


Fig. 12. Exposure map for NGC 3384

Additionally, merged exposure maps of the 0.5-7 keV band are shown for NGC 3115 and NGC 4452.

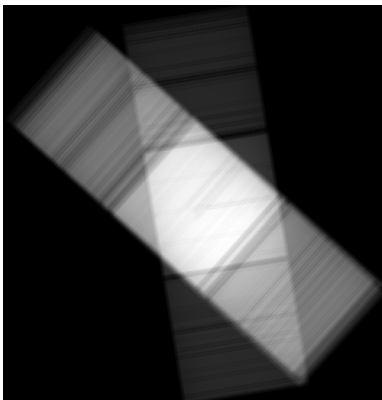


Fig. 13. Exposure Map for NGC 4452

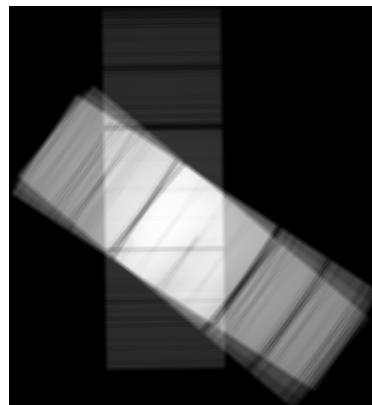


Fig. 14. Exposure Map for NGC 3115

During the binning process, I developed many graphs before the one shown in my paper. This included the development of comparison and combination graphs. If you compare these graphs to the final graph in the paper, you can see how the binning process was refined over time.

Fig. 15. Combination graph of various galaxies Luminosity vs Photon Index (Γ)

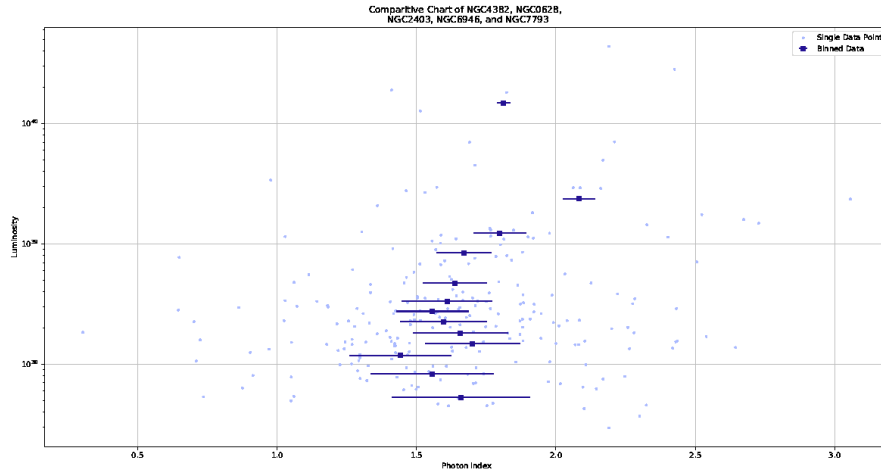
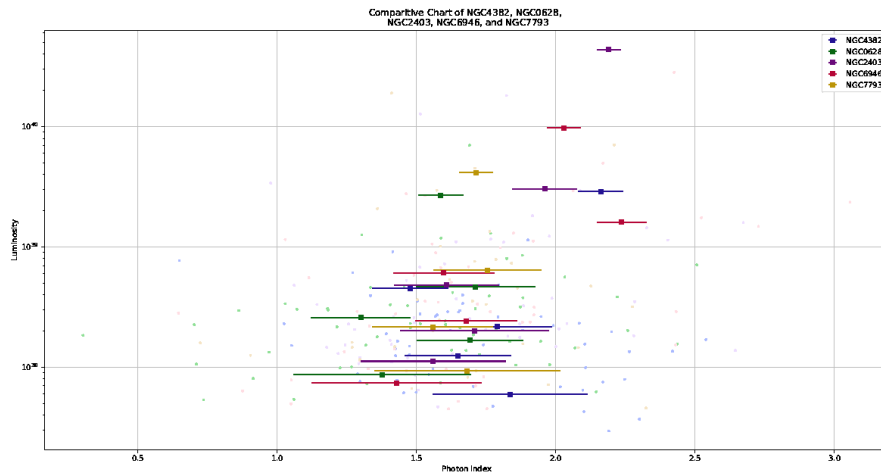


Fig. 16. Comparative graph of various galaxies Luminosity vs Photon Index (Γ)



As the binning process was refined, the error bars decreased. In addition, the distinctness between results from different galaxies decreased. However, due to a lack of data in many individual galaxies, the combination was the one of main relevance by the end of the study.

spectral_analysis.py

```
#!/usr/bin/python

import os
import math
import matplotlib.pyplot as plt
import numpy
from numpy import sin, pi, arange
import astropy.io
from astropy.io import fits
from PIL import Image

def main():

    fits_file = []

    #set to the directory containing all data you wish to plot
    fits_dir = os.listdir(os.environ["RESEARCH_DATA_PATH"] + "/Final-fits/")

    #specify the path each data file
    for i in range(len(fits_dir)):
        fits_file.append(os.environ["RESEARCH_DATA_PATH"] + "/Final-fits/" + fits_dir[i])

    print(fits_file)
    fig = plt.figure(figsize=(20, 10))
    ax1 = fig.add_subplot(111)

    x = []
    x_error = []
    x_error_mean = []
    y = []

    for iterator, value in enumerate(fits_file):
        hdu_list = fits.open(value)

        #our data is now put into columns
        data = hdu_list[1].data
        cols = hdu_list[1].columns
        hdu_list.close()

        #take the values you need. If you need a new field, use print(cols) and use
        gamma = data.field('gamma')
        gamma_error = data.field('gamma_err')
        # print(gamma_error)
        lh8 = data.field('lh8')

        #gamma of value 1.7 is an error as is NaN, so we only append indexes without
        #those values
        gamma_indices = numpy.where(gamma != 1.7)

        for i, value in enumerate(gamma_indices[0]):
            if (gamma[value] == gamma[value] and lh8[value] == lh8[value]
                and gamma_error[value] > 0):
                x.append(gamma[value])
                x_error.append(gamma_error[value])
                y.append(lh8[value])

    #this guy holds our data set sorted by luminosity
    data_set = []
    for i in range(len(x)):
        temp = [y[i], x[i], x_error[i]]
        data_set.append(temp)

    #sort it
    data_set.sort(key=lambda x: x[0])

    Ay = []
    Ax = []
    Ax_error = []

    for i in range(len(x)):
        Ay.append(data_set[i][0])
```

```

    Ax.append(data_set[i][1])
    Ax_error.append(data_set[i][2])

bin_minimum = Ay[0]
#Set this in case you're binning too many values
bin_upper_limit = 50
bin_lower_limit = 15

y_binned = []
x_binned = []
x_error_binned = []

y_unbinned = []
x_unbinned = []
x_error_unbinned = []

counter = []

# THE BELOW CODE AUTOBINS NORMALLY #
j = 0
for i in range(len(Ay)):
    if(j == len(x_error_binned) - 1):
        if((numpy.sqrt(x_error_binned[j])/(counter[j]) < 0.1) and (
            counter[j] >= bin_lower_limit)):
            j += 1
        elif(counter[j] >= bin_upper_limit):
            j += 1
        else:
            counter[j] += 1
            y_binned[j] += Ay[i]
            x_binned[j] += Ax[i]
            x_error_binned[j] += Ax_error[i]**2
    else:
        y_binned.append(0)
        x_binned.append(0)
        x_error_binned.append(0)
        counter.append(0)

        counter[j] += 1
        y_binned[j] += Ay[i]
        x_binned[j] += Ax[i]
        x_error_binned[j] += Ax_error[i]**2
# END AUTOBIN CODE#

#calculates the mean error as sqrt(sum(errors^2))/sqrt(n)
for j in range(len(y_binned)):
    if value == value:
        y_binned[j] = y_binned[j]/counter[j]
        x_binned[j] = x_binned[j]/counter[j]
        x_error_binned[j] = numpy.sqrt(x_error_binned[j])/(counter[j])

no = '_nolegend_'

#all following code is for plotting to our figure
ax1.scatter(x, y, color = '#aabaff', zorder = 2, s=5)
ax1.errorbar(x_binned, y_binned, xerr = x_error_binned, color = '#231193', fmt = 'o',
            marker = "s", zorder = 4)
ax1.errorbar(x_unbinned, y_unbinned, xerr = x_error_unbinned, color = '#3219cd', fmt
            = 'o', zorder = 3, label = no, ms=3)

#test script
# ax1.scatter(x, y, color = '#e6e6e6', zorder = 1, label = no, s=5)
# ax1.errorbar(x_binned, y_binned, xerr = x_error_binned, color = '#e6e6e6', fmt = '.',
            marker = "s", zorder = 1, label = no)
# ax1.errorbar(x_unbinned, y_unbinned, xerr = x_error_unbinned, color = '#e6e6e6',
            fmt = '.', zorder = 1, label = no)

plt.yscale('log');
ax1.set_xlabel("Photon Index")
ax1.set_ylabel("Luminosity")
ax1.set_title(r'Luminosity vs Photon Index ($\Gamma$) of NGC4382, NGC0628, NGC2403,
```

```
NGC6946, NGC7793, NGC2841, NGC3184, NGC3198, NGC4559, M63, M94, M95, and M100')
legend_labels = ["Single Data Point", "Binned Data"]

ax1.legend(legend_labels)

plt.grid(True)
plt.draw()
ax1.apply_aspect()

#test script
# fig.savefig('alt_name.eps', dpi=fig.dpi)
# Image.open('alt_name.eps').save('alt_name.png', 'png')

fig.savefig('combination_auto_update.eps', dpi=fig.dpi)
Image.open('combination_auto_update.eps').save('combination_auto_update.png', 'png')
plt.show()

return 0
main()
```